

Electron transport in nodal-line semimetals

S.V. Syzranov^{1,2} and B. Skinner³

¹Joint Quantum Institute, NIST/University of Maryland, College Park, MD 20742, USA

²School of Physics and Astronomy, Monash University, Victoria 3800, Australia

³Massachusetts Institute of Technology, Cambridge, MA 02139 USA

(Dated: December 28, 2016)

We study the electrical conductivity in a nodal-line semimetal with charged impurities. The screening of the Coulomb potential in this system is qualitatively different from what is found in conventional metals or semiconductors, with the screened potential ϕ decaying as $\phi \propto 1/r^2$ over a wide interval of distances r . This unusual screening gives rise to a rich variety of conduction regimes as a function of temperature, doping level and impurity concentration. In particular, nodal-line semimetals exhibit a diverging mobility $\propto 1/|\mu|$ in the limit of vanishing chemical potential μ , a linearly-increasing dependence of the conductivity on temperature, $\sigma \propto T$, and a large weak-localization correction with a strongly anisotropic dependence on magnetic field.

A topological semimetal is a semimetal in which the conduction and valence bands touch at a point or a line (the nodal line) in momentum space. The most well-known examples are Weyl^{1–6}, nodal-line^{7,8} and parabolic⁹ semimetals. Such materials have been in the focus of researchers' attention since their discovery several years ago, owing to the abundance of novel fundamental phenomena predicted in them, including the chiral anomaly¹⁰, topologically protected Fermi arcs^{1,3,6}, and unconventional disorder-driven transitions^{11,12}.

In the presence of disorder, topological semimetals may display a rich variety of electrical conduction regimes, depending on the nature of quenched disorder, temperature, and doping level. For example, these systems may exhibit metallic or insulating transport properties or unconventional dependencies of the conductivity on temperature. In general, transport in topological semimetals is determined by the behaviour of several potentially competing factors at energies near the band touching, including the vanishing density of states (in the disorder-free limit), divergence of the screening length and the behaviour of the elastic scattering rate.

Although the conductivity of Weyl semimetals has received considerable attention in the literature, other types of semimetals have largely evaded researchers' attention. In this paper we study the conductivity of a three-dimensional (3D) nodal-line semimetal (NLS), where the conduction and valence bands touch along a line in momentum space, as in the recently discovered ZrSiS⁷, HfSiS¹³ and PbTaSe₂⁸ (a number of other materials have also been predicted to be NLSs^{14–21}). We calculate the NLS conductivity microscopically and study its dependence on temperature, doping level and impurity concentration for realistically achievable regimes. We demonstrate that the Coulomb interaction in a low-doped NLS is only partially screened and has the distance dependence $\propto 1/r^2$ across a broad interval of r , which leads to qualitatively new features in conduction and a richer variety of transport regimes as compared to other semimetals, semiconductors and metals. In particular, NLSs display divergent quasiparticle mobility in the limit of vanishing doping, linear dependence of con-

ductivity on temperature and large weak-localisation corrections to the conductivity with a strongly anisotropic dependence on magnetic field.

Model. It may be assumed normally that in an undoped NLS all points of the nodal line lie at the Fermi energy. In a doped material, where a finite carrier concentration is provided either by donor or acceptor impurities or by additional pockets of states, the Fermi surface has the shape of a tube surrounding the nodal line, as depicted in Fig. 1a. For realistic doping levels, the radius of the tube (the Fermi momentum) is significantly smaller than the characteristic size of the nodal line, which is typically of order of the inverse lattice spacing.

We also assume that the dominant source of momentum scattering for quasiparticles is provided by Coulomb impurities, as is typical for semiconductors and semimetals. Due to the long-range nature of the potential of these impurities, they provide only small-momentum scatter-

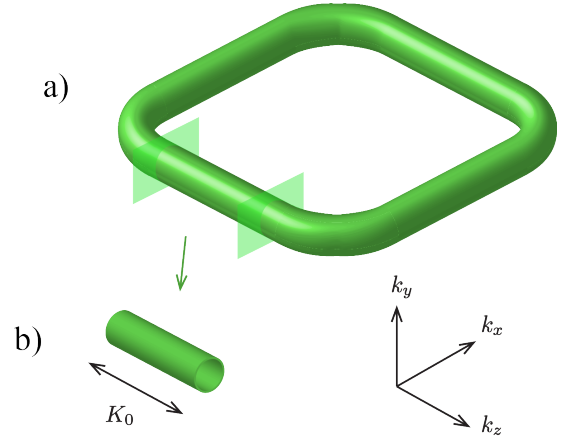


FIG. 1. (Colour online) Fermi surface (FS) in a doped NLS. a) FS for a closed nodal line. b) A straight segment of the FS. For a long-range-correlated disorder potential, characteristic of Coulomb impurities, the momentum scattering along the nodal line is small, and the line may be approximated by a chain of straight segments. The total conductivity is given by the sum of the segment contributions.

ing relative to the diameter of the nodal line, so that the curvature of the nodal line may be neglected in each scattering event. Scattering processes between opposite sides of the nodal line can also be neglected.

The Hamiltonian for a quasiparticle near a short straight segment of the nodal line is given by

$$\hat{\mathcal{H}}_0 = v(\hat{\sigma}_x k_x + \hat{\sigma}_y k_y) + \xi(k_z) + e\phi(\mathbf{r}), \quad (1)$$

where k_x and k_y are the transverse momentum components (hereinafter $\hbar = 1$); $\hat{\sigma}_x$ and $\hat{\sigma}_y$ are Pauli matrices in the space of a spin-1/2 degree of freedom (pseudospin space); v is the velocity of transverse motion, which for simplicity is assumed to be the same in the x and y directions throughout this paper; $\xi(k_z)$ is the contribution of the longitudinal motion to the kinetic energy; and $\phi(\mathbf{r})$ is the electric potential created by charged impurities screened by electrons.

For the small quasiparticle energies under consideration the longitudinal quasiparticle velocity may be estimated as $v_z \simeq vk_z/p_0$, and it is strongly suppressed compared to the transverse velocity v , where p_0 is the local radius of curvature of the nodal line (in momentum space). As a result, the quasiparticle dynamics on sufficiently short length scales is effectively 2D and is confined to the plane perpendicular to the segment of the nodal line under consideration.

The strength of the Coulomb interaction in an NLS may be characterised by the effective fine structure constant $\alpha = \frac{e^2}{\varkappa v}$ (in Gaussian units), with \varkappa being the dielectric constant. Usually $\alpha \lesssim 1$ in semimetals (see, e.g., Refs. 22 and 23 for estimates). In this paper we assume for simplicity that $\alpha \ll 1$, which allows one to use the linear Poisson equation to describe the electrostatic potential $\phi(\mathbf{r})$ created by screened charged impurities:

$$\varkappa \nabla^2 \phi(\mathbf{r}) + 4\pi e^2 \int \Pi(\mathbf{r}, \mathbf{r}') \phi(\mathbf{r}') d\mathbf{r}' = -4\pi e \sum_j Z_j \delta(\mathbf{r} - \mathbf{r}_j). \quad (2)$$

Here, \mathbf{r}_j and $Z_j e$ are the location and the charge of the j th impurity (for donors and acceptors $Z_j = \pm 1$, respectively) and $\Pi(\mathbf{r}, \mathbf{r}') = -i \int_{-\infty}^0 \langle [\hat{n}(0, \mathbf{r}), \hat{n}(t', \mathbf{r}')] \rangle dt'$ is the zero-frequency polarisation operator, which describes the linear response of the local density of electrons $\hat{n}(\mathbf{r})$ to the electrostatic potential $\phi(\mathbf{r}')$.

Polarisation operator. Due to the effectively two-dimensional short-distance dynamics of the quasiparticles, the screening properties of electrons near a short segment of the nodal line are related to those in graphene^{24,25}, with the contribution to the polarisation operator given by that of 2D Dirac electrons multiplied by $gK_{\parallel}/(2\pi)$, where g indicates the spin and valley degeneracy and K_{\parallel} is the length of this segment in momentum space. The full polarisation operator is given by a sum of all such straight-line-segment contributions, since the entire nodal line may be approximated as a chain of straight-line segments.

At low temperature and chemical potential the polarisation operator $\Pi(\mathbf{q})$ is linear in the momentum $|\mathbf{q}|$ for any direction of \mathbf{q} . While the constant of proportionality between $\Pi(\mathbf{q})$ and $|\mathbf{q}|$ for a given direction of $|\mathbf{q}|$ depends in general on the shape of the nodal line²⁶, below we assume for simplicity that the full polarisation operator is isotropic in \mathbf{q} . For sufficiently high chemical potentials μ or temperatures T , $\Pi(\mathbf{q})$ is momentum-independent and is determined by the density of states (DoS) at energies $\sim \max(|\mu|, T)$. Thus, the behaviour of the polarisation operator in an NLS in the limits of high and low temperatures may be summarised as

$$\Pi(\mathbf{q}) = \begin{cases} -gCK_{\circ}|\mathbf{q}|/v, & v|\mathbf{q}| \gg T, |\mu|, \\ -gK_{\circ}|\mu|/(4\pi^2 v^2), & |\mu| \gg T, v|\mathbf{q}|, \\ -gK_{\circ}T \ln 2/(2\pi^2 v^2), & T \gg |\mu|, v|\mathbf{q}|. \end{cases} \quad (3)$$

Here, K_{\circ} is the length of the nodal line and C is a constant of order unity, which accounts for the details of the geometry of the nodal line.

Screened impurity potential. At low temperature and chemical potential, the distance dependence of the screened Coulomb potential in an NLS is qualitatively different from that in conventional metals, dielectrics, or other semimetals. The Fourier transform of the screened interaction is given by $\phi(\mathbf{q}) = \phi_0(\mathbf{q}) [1 - \Pi(\mathbf{q})\phi_0(\mathbf{q})]^{-1}$, where $\phi_0(\mathbf{q}) = 4\pi e^2/(\varkappa q^2)$ describes the unscreened Coulomb interaction and the polarisation operator $\Pi(\mathbf{q})$ is given by Eq. (3). At short

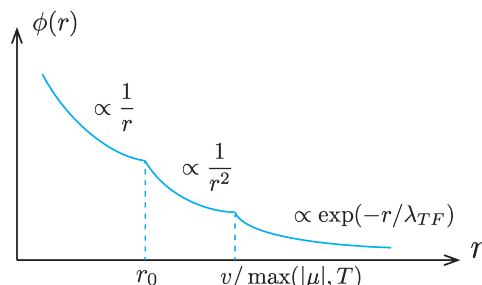


FIG. 2. (Colour online) Screened Coulomb interaction as a function of distance at low temperatures and doping levels.

distances the interaction is unscreened, $\phi(r) \simeq e^2/(\varkappa r)$. At distances of order of

$$r_0 = (\alpha g K_{\circ})^{-1} \quad (4)$$

the interaction potential crosses over to the unconventional form

$$\phi(r) = \frac{e^2 r_0}{2\pi^2 \varkappa C} \frac{1}{r^2}. \quad (5)$$

Finally, at very large distances, exceeding the characteristic wavelength $\max(|\mu|, T)/v$ of the quasiparticles in the conduction (valence) band, the polarisation operator is effectively local, $\Pi(\mathbf{r}, \mathbf{r}') \approx -(4\pi e^2 \lambda_{TF}^2 / \varkappa)^{-1} \delta(\mathbf{r} -$

\mathbf{r}'), resulting in the exponentially suppressed interaction $\phi(r) \propto \exp(-r/\lambda_{\text{TF}})$. Here we have introduced the Thomas-Fermi (TF) screening length, given by

$$\lambda_{\text{TF}}^{-2} = \begin{cases} (g\alpha/\pi) \cdot K_{\circ}|\mu|/v, & |\mu| \gg T, \\ (2g\alpha/\pi) \ln 2 \cdot K_{\circ}T/v, & T \gg |\mu|. \end{cases} \quad (6)$$

The dependence of the screened interaction on distance is summarised in Fig. 2, assuming low temperature and chemical potential ($|\mu|, T \ll \alpha g v K_{\circ}$).

For high temperatures or chemical potentials, $\max(|\mu|, T) \gg \alpha g v K_{\circ}$, the characteristic quasiparticle wavelength becomes shorter than the distance r_0 , and the intermediate regime with $\phi(r) \propto 1/r^2$ (see Fig. 2) vanishes. In this case the screened electrostatic potential is given by

$$\phi(r) = \frac{e^2}{\kappa r} \exp(-r/\lambda_{\text{TF}}) \quad (7)$$

across all distances, as in a conventional metal²⁷.

Quasiparticle scattering. As mentioned in the introduction, it is possible to approximate the nodal line by a chain of straight-line segments and to consider separately the quasiparticle transport near each segment. Due to the suppressed quasiparticle motion along the nodal line, the transverse conductivity σ_x of a given segment with momentum length K_{\parallel} significantly exceeds its longitudinal conductivity σ_z . The sum of the conductivity from all segments, with their various orientations, is then of order of $\sigma_x K_{\circ}/K_{\parallel}$.

The relaxation of the momentum of quasiparticles with energy ε (transverse momentum ε/v) near a straight segment of the nodal line due to elastic scattering off impurities is characterised by the transport scattering time τ_{tr} . In the Born approximation,

$$\frac{1}{\tau_{\text{tr}}(\varepsilon)} = 2\pi n_{\text{imp}} \int \frac{d\mathbf{p}}{(2\pi)^3} |\phi(\mathbf{p} - \mathbf{k}) \langle \sigma_{\mathbf{p}} | \sigma_{\mathbf{k}} \rangle|^2 (1 - \cos \theta_{\mathbf{k}, \mathbf{p}}) \delta(kv - pv), \quad (8)$$

where n_{imp} is the total concentration of (donor and acceptor) impurities, \mathbf{k} is a momentum with the transverse component ε/v , $\phi(\mathbf{q})$ is the Fourier-transform of the impurity potential, and $|\sigma_{\mathbf{p}}\rangle$ is the pseudospin state of a quasiparticle with momentum \mathbf{p} in a given (conduction or valence) band; $|\langle \sigma_{\mathbf{p}} | \sigma_{\mathbf{k}} \rangle|^2 = (1 + \cos \theta_{\mathbf{k}, \mathbf{p}})/2$, with $\theta_{\mathbf{k}, \mathbf{p}}$ being the angle between the transverse components of \mathbf{k} and \mathbf{p} .

Low doping levels. At low doping, $|\mu| \ll \alpha g v K_{\circ}$, and zero temperature, the Fermi wavelength $\sim \mu/v$ significantly exceeds the length scale r_0 [Eq. (4)]. Thus, the scattering of quasiparticles at the Fermi surface is determined by the $\propto 1/r^2$ tail of the impurity potential rather than the $\propto 1/r$ core (see Fig. 2).

Using Eqs. (5) and (8), we find the transport scattering time in this regime to be (see Supplemental Material for details)

$$\tau_{\text{tr}} = \gamma_{\text{tr}} g^2 K_{\circ}^2 / (n_{\text{imp}} v), \quad (9)$$

where γ_{tr} is a non-universal constant of order unity, which depends on the details of the geometry of the nodal line. We note that typical scattering events have large scattering angles $\theta_{\mathbf{p}, \mathbf{k}} \sim 1$, and therefore the transport scattering time (9) is of the same order as the typical time τ_0 between collisions (the elastic scattering time).

For weak disorder, such that $\tau_0 \mu \gg 1$, the DoS of quasiparticles at the Fermi energy is weakly affected by impurities, and the conductivity is dominated by the Drude contribution²⁷⁻²⁹, which takes into account quasiparticle scattering processes not involving quasiparticle interference. The transverse Drude conductivity of the straight nodal-line segment is given by

$$\sigma_x(\mu) = \frac{1}{2} \frac{K_{\parallel}}{2\pi} g e^2 v^2 \nu_{2D}(\mu) \tau_{\text{tr}} = \frac{\gamma_{\text{tr}}}{8\pi^2} \frac{g^3 e^2 K_{\circ}^2 K_{\parallel} |\mu|}{n_{\text{imp}} v}, \quad (10)$$

where $\nu_{2D} = \frac{|\mu|}{2\pi v^2}$ is the quasiparticle DoS (per spin per valley) in the transverse 2D plane. As discussed above, the conductivity of the entire NLS is of order (10) with the replacement $K_{\parallel} \rightarrow K_{\circ}$.

Since the concentration of charge carriers depends quadratically on the chemical potential, $n(\mu) \propto \mu^2$, Eq. (10) implies that the quasiparticle mobility $\frac{\sigma_x(\mu)}{en(\mu)} \propto \frac{1}{|\mu|}$ diverges as the chemical potential approaches the nodal line, even for a fixed impurity concentration.

Temperature dependence. In the regime of low doping under consideration ($|\mu| \ll \alpha g v K_{\circ}$), the conductivity strongly depends on temperature when $T \gg |\mu|$ (here we neglect electron-phonon scattering and the interaction between quasiparticles). In the limit of weak disorder, we find for the conductivity of a straight segment of the nodal line

$$\sigma_x(T \gg |\mu|) = - \int n'_{\text{F}}(\varepsilon) \sigma_x(\varepsilon) d\varepsilon = \frac{\gamma_{\text{tr}} \ln 2}{4\pi^2} \frac{g^2 e^2 K_{\circ}^2 K_{\parallel}}{n_{\text{imp}} v} T, \quad (11)$$

where $n_{\text{F}}(\varepsilon) = 1/[\exp(\varepsilon/T) + 1]$ is the Fermi distribution function and $\sigma_x(\varepsilon)$ is given by Eq. (10). The conductivity of the NLS is described approximately by Eq. (11) with the replacement $K_{\parallel} \rightarrow K_{\circ}$. The linear-in- T dependency of the conductivity comes from thermally activated charge carriers with a linear density of states $\nu(\varepsilon) \propto \varepsilon$ and a constant scattered rate (9).

High-doping regime. When the NLS is so heavily doped that $|\mu| \gg \alpha g v K_{\circ}$, the TF screening radius becomes shorter than r_0 and the screened potential is equivalent to that in a conventional metal [Eq. (7)]. In this regime the transport properties of the NLS are also similar to those of a conventional metal and, in particular, weakly dependent on the temperature. Using Eqs. (7) and (8) we find the transport scattering rate in this regime³⁰

$$\frac{1}{\tau_{\text{tr}}(\varepsilon)} = \frac{2\pi \alpha^2 v^3 n_{\text{imp}}}{\varepsilon^2} \ln \frac{|\varepsilon| \lambda_{\text{TF}}}{v}. \quad (12)$$

At such high doping the impurities typically scatter quasiparticle momenta by small angles $\theta \ll 1$, which

leads to a significantly shorter elastic scattering time $\tau_0 = (4\pi\alpha^2 n_{\text{imp}} v \lambda_{\text{TF}}^2)^{-1}$ (see Supplemental Material for details). The Drude conductivity of a highly-doped NLS is then given by the segment contribution

$$\sigma_x(\mu) = \frac{gK_{\parallel} e^2 |\mu|^3}{8\pi^3 \alpha^2 v^3 n_{\text{imp}} \ln[|\mu|/(\alpha g K_{\circ} v)]}, \quad (13)$$

with K_{\parallel} replaced by a quantity of order K_{\circ} .

Weak localisation. For all doping levels, the quasiparticle dynamics on sufficiently short length scales are effectively 2D and are confined to the plane perpendicular to the nodal line. One can therefore expect significant quantum interference effects that are typical of 2D systems^{28,31}. In order to estimate the characteristic length scale l_{dim} below which these interference effects are strong, we assume that the quasiparticles have a small longitudinal dispersion $\xi(k_z) = vk_z^2/2p_0$, *e.g.*, due to the curvature of the nodal line (in which case p_0 is the local radius of curvature of the line).

To estimate l_{dim} , let us consider a quasiparticle whose momentum \mathbf{k} at time $t = 0$ lies in the x - y plane. Due to the small dispersion in the z direction and collisions with impurities, such a quasiparticle slowly drifts away from the x - y plane. During each collision with an impurity, the longitudinal velocity of the quasiparticle changes by an amount $\delta v_z \sim \pm vk/K_{\circ}$, where we have assumed that the local radius p_0 of the nodal line is of order K_{\circ} . After a long time $t \gg \tau_0$, the total change in z velocity is of order $\Delta v_z \sim (vk/K_{\circ})\sqrt{t/\tau_0}$, and the quasiparticle travels a distance $\Delta z \sim t\Delta v_z \sim (vk/K_{\circ})\sqrt{t^3/\tau_0}$ in the z direction. When this drift length exceeds the electron wavelength $\sim k^{-1} = v/|\mu|$, the quasiparticle can be considered to have “escaped” its initial 2D plane of motion and no longer participates in the 2D interference effects in this plane. The characteristic time of 2D interference can thus be estimated as $t_{\text{dim}} \sim (v^2 K_{\circ}^2 \tau_0 / \mu^4)^{\frac{1}{3}}$, which corresponds to the length

$$l_{\text{dim}} = (v^4 K_{\circ} / \mu^2)^{\frac{1}{3}} \tau_{\text{tr}}^{\frac{1}{2}} \tau_0^{\frac{1}{6}} \quad (14)$$

of diffusion in the initial 2D plane.

Thus, quantum interference effects in an NLS on short distances $L < l_{\text{dim}}$ are equivalent to those of 2D Dirac fermions, such as electrons in graphene in a single valley, which exhibit weak-antilocalisation (WAL) corrections to conductivity^{32,33}. On larger length scales $L > l_{\text{dim}}$, the classical trajectories of the quasiparticles are essentially 3D and the interference between them is suppressed. Thus, the conductivity of the NLS receives a WAL correction

$$\delta\sigma_{WL} = \frac{ge^2 K_{\circ}}{(2\pi)^3} \times \begin{cases} \ln[\min(l_{\phi}, l_{\text{dim}})/(v\tau_{\text{tr}})], & B \ll B_0, \\ \tilde{\gamma}_B(\mathbf{n}_B) \cdot \ln[l_B/(v\tau_{\text{tr}})], & B \gg B_0, \end{cases} \quad (15)$$

where $B_0 = \frac{c}{ev\tau_{\text{tr}} \min(l_{\phi}, l_{\text{dim}})}$ is the characteristic value of magnetic field at which the WAL is affected by the field, $\tilde{\gamma}_B(\mathbf{n}_B) < 1$ is a non-universal coefficient depending on

the geometry of the nodal line and the direction $\mathbf{n}_B = \mathbf{B}/B$ of the magnetic field, l_{ϕ} is the dephasing length, and $l_B = \frac{c}{ev\tau_{\text{tr}}B}$.

The first line in Eq. (15) describes the conventional WAL corrections due to the interference of 2D Dirac fermions^{32,33}; the second line describes the partial suppression of WAL by magnetic field. Because the correction is dominated by effectively 2D interference effects, the magnetic field \mathbf{B} does not suppress the interference near parts of the nodal line perpendicular to \mathbf{B} (here we neglect the much weaker effect of magnetic field on the motion along the nodal line), and therefore the suppression of the WAL correction by magnetic field strongly depends on the direction of the field. In particular, if the entire nodal line lies in one plane, as, for example, in ZrSiS (see Fig. 1a), the in-plane magnetic field can partially suppress the WAL correction, while the field perpendicular to the plane has no significant effect. We note also that for sufficiently weak disorder ($\mu\tau_{\text{tr}} \gg 1$) the conductivity is dominated by the Drude contribution (10), and the interference correction (15) is negligible.

Summary and discussion. We have studied the conductivity in a weakly disordered NLS with charged impurities. At low temperature and chemical potential, the screened electrostatic interaction is qualitatively different from that in conventional semiconductors and semimetals and includes a broad regime of distances for which $\phi(r) \propto 1/r^2$ (see Fig. 2). Such screening of impurities can potentially be probed directly by scanning tunnelling microscopy, and it also manifests itself in the dependencies of the conductivity on temperature and doping level.

In particular, a low-doped NLS exhibits divergent quasiparticle mobility $\propto |\mu|^{-1}$ at vanishing chemical potential μ , with conductivity given by Eq. (10). In this regime, the NLS also exhibits strong temperature dependence of the conductivity, $\sigma(T) \propto T$, at $T \gg |\mu|$. At larger doping, the impurities are strongly screened, and the transport properties of the NLS resemble those of a conventional metal.

In all of these regimes the conductivity of an NLS receives large WAL corrections [Eq. (15)] due to the suppressed motion of the charge carriers along the nodal line, which makes electron dynamics effectively 2D on short scales and thus leads to strong single-particle interference effects.

For presently existing NLSs, which have K_{\circ} of order 1 \AA^{-1} and v of order 10^8 cm/s , the energy scale $agvK_{\circ}$ is as large as several eV for $\alpha \sim 0.1$. Existing NLS materials are therefore likely to fall in the “low doping” regime of our analysis. Recent experiments on ZrSiS^{34–37}, for example, report μ of order several hundred meV. In this case Eq. (10) implies a low-temperature resistivity on the order of tens of $\text{n}\Omega \cdot \text{cm}$, assuming a charged impurity concentration of order 10^{19} cm^{-3} (as reported in Ref. 37). This is consistent with the experimental measurements in Refs. 34 and 36.

Finally, we note that current experiments correspond to the regime of weak disorder ($\mu\tau_0 \gg 1$), which is as-

sumed throughout this paper and which requires $n_{\text{imp}} \ll g^2 K_o^2 |\mu|/v \sim 10^{21} \text{ cm}^{-3}$. Since there is no localisation in systems of effectively-2D Dirac fermions (in the absence of scattering between opposite ends of the nodal line), one can expect that stronger disorder ($n_{\text{imp}} \gg g^2 K_o^2 |\mu|/v$) may lead to a universal minimal conductivity $\sigma \sim e^2 K_o$ in an NLS. However, this regime of strong disorder is left for a future study. Another question, which deserves further investigation, is the role of the interaction between quasiparticles in transport, as for sufficiently high temperatures the NLS resistivity will be dominated by the scattering of quasiparticles on each other rather than impurity scattering.

Acknowledgements. We are grateful to M.S. Fuhrer, B. Weber and especially Ya.I. Rodionov for valuable discussions. SVS was financially supported by AFOSR, NSF QIS, ARO MURI, ARO, ARL CDQI and NSF PFC at Joint Quantum Institute. BS was supported as part of the MIT Center for Excitonics, an Energy Frontier Research Center funded by the U.S. Department of Energy, Office of Science, Basic Energy Sciences under Award no. DE-SC0001088. SVS also acknowledges the hospitality of School of Physics and Astronomy at Monash University and of the MIT Center for Excitonics, where parts of this work were completed.

-
- ¹ Xiangang Wan, Ari M. Turner, Ashvin Vishwanath, and Sergey Y. Savrasov, "Topological semimetal and Fermi-arc surface states in the electronic structure of pyrochlore iridates," *Phys. Rev. B* **83**, 205101 (2011).
 - ² Shin-Ming Huang, Su-Yang Xu, Ilya Belopolski, Chi-Cheng Lee, Guoqing Chang, BaoKai Wang, Nasser Alidoust, Guang Bian, Madhab Neupane, Chenglong Zhang, Shuang Jia, Arun Bansil, Hsin Lin, and M. Zahid Hasan, "A Weyl Fermion semimetal with surface Fermi arcs in the transition metal mononpnictide TaAs class," *Nature Comm.* **6**, 7373 (2015).
 - ³ Su-Yang Xu, Ilya Belopolski, Nasser Alidoust, Madhab Neupane, Guang Bian, Chenglong Zhang, Raman Sankar, Guoqing Chang, Zhujun Yuan, Chi-Cheng Lee, Shin-Ming Huang, Hao Zheng, Jie Ma, Daniel S. Sanchez, BaoKai Wang, Arun Bansil, Fangcheng Chou, Pavel P. Shibayev, Hsin Lin, Shuang Jia, and M. Zahid Hasan, "Discovery of a Weyl fermion semimetal and topological Fermi arcs," *Science* **349**, 6248 (2015).
 - ⁴ Su-Yang Xu, Ilya Belopolski, Daniel S. Sanchez, Chenglong Zhang, Guoqing Chang, Cheng Guo, Guang Bian, Zhujun Yuan, Hong Lu, Tay-Rong Chang, Pavel P. Shibayev, Mykhailo L. Prokopovych, Nasser Alidoust, Hao Zheng, Chi-Cheng Lee, Shin-Ming Huang, Raman Sankar, Fangcheng Chou, Chuang-Han Hsu, Horng-Tay Jeng, Arun Bansil, Titus Neupert, Vladimir N. Strocov, Hsin Lin, Shuang Jia, and M. Zahid Hasan, "Experimental discovery of a topological Weyl semimetal state in TaP," *Sci. Adv.* **1**, 1501092 (2015).
 - ⁵ Su-Yang Xu, Nasser Alidoust, Ilya Belopolski, Zhujun Yuan, Guang Bian, Tay-Rong Chang, Hao Zheng, Vladimir N. Strocov, Daniel S. Sanchez, Guoqing Chang, Chenglong Zhang, Daixiang Mou, Yun Wu, Lunan Huang, Chi-Cheng Lee, Shin-Ming Huang, BaoKai Wang, Arun Bansil, Horng-Tay Jeng, Titus Neupert, Adam Kaminski, Hsin Lin, Shuang Jia, and M. Zahid Hasan, "Discovery of a Weyl fermion state with Fermi arcs in niobium arsenide," *Nat. Phys.* **11**, 748 (2015).
 - ⁶ B. Q. Lv, H. M. Weng, B. B. Fu, X. P. Wang, H. Miao, J. Ma, P. Richard, X. C. Huang, L. X. Zhao, G. F. Chen, Z. Fang, X. Dai, T. Qian, and H. Ding, "Experimental discovery of Weyl semimetal TaAs," *Phys. Rev. X* **5**, 031013 (2015).
 - ⁷ Leslie M. Schoop, Mazhar N. Ali, Carola Stra er, Andreas Topp, Andrei Varykhalov, Dmitry Marchenko, Viola Dupel, Stuart S. P. Parkin, Bettina V. Lotsch, and Christian R. Ast, "Dirac cone protected by non-symmorphic symmetry and three-dimensional Dirac line node in ZrSiS," *Nat. Comm.* **7**, 11696 (2016).
 - ⁸ Guang Bian, Tay-Rong Chang, Raman Sankar, Su-Yang Xu, Hao Zheng, Titus Neupert, Ching-Kai Chiu, Shin-Ming Huang, Guoqing Chang, Ilya Belopolski, Daniel S. Sanchez, Madhab Neupane, Nasser Alidoust, Chang Liu, BaoKai Wang, Chi-Cheng Lee, Horng-Tay Jeng, Chenglong Zhang, Zhujun Yuan, Shuang Jia, Arun Bansil, Fangcheng Chou, Hsin Lin, and M. Zahid Hasan, "Topological nodal-line fermions in spin-orbit metal PbTaSe2," *Nat. Comm.* **7**, 10556 (2016).
 - ⁹ Takeshi Kondo, M. Nakayama, R. Chen, J. J. Ishikawa, E.-G. Moon, T. Yamamoto, Y. Ota, W. Malaeb, H. Kanai, Y. Nakashima, Y. Ishida, R. Yoshida, H. Yamamoto, M. Matsunami, S. Kimura, N. Inami, K. Ono, H. Kumigashira, S. Nakatsuji, L. Balents, and S. Shin, "Quadratic Fermi node in a 3D strongly correlated semimetal," *Nature Communications* **6**, 10042 (2015).
 - ¹⁰ S. A. Parameswaran, T. Grover, D. A. Abanin, D. A. Pesin, and A. Vishwanath, "Probing the chiral anomaly with non-local transport in three-dimensional topological semimetals," *Phys. Rev. X* **4**, 031035 (2014).
 - ¹¹ E. Fradkin, "Critical behavior of disordered degenerate semiconductors. i. models, symmetries, and formalism," *Phys. Rev. B* **33**, 3257 (1986).
 - ¹² See Ref. 38 for a review.
 - ¹³ D. Takane, Zhiwei Wang, S. Souma, K. Nakayama, C. X. Trang, T. Sato, T. Takahashi, and Yoichi Ando, "Dirac-node arc in the topological line-node semimetal HfSiS," *Phys. Rev. B* **94**, 121108 (2016).
 - ¹⁴ A. A. Burkov, M. D. Hook, and Leon Balents, "Topological nodal semimetals," *Phys. Rev. B* **84**, 235126 (2011).
 - ¹⁵ Youngkuk Kim, Benjamin J. Wieder, C. L. Kane, and Andrew M. Rappe, "Dirac line nodes in inversion-symmetric crystals," *Phys. Rev. Lett.* **115**, 036806 (2015).
 - ¹⁶ Lilia S. Xie, Leslie M. Schoop, Elizabeth M. Seibel, Quinn D. Gibson, Weiwei Xie, and Robert J. Cava, "A new form of Ca3P2 with a ring of Dirac nodes," *APL Mat.* **3**, 083602 (2015).
 - ¹⁷ Chen Fang, Yige Chen, Hae-Young Kee, and Liang Fu, "Topological nodal line semimetals with and without spin-orbital coupling," *Phys. Rev. B* **92**, 081201(R) (2015).
 - ¹⁸ L.-Y. Gan, R. Wang, Y. J. Jin, D. B. Ling, J. Z. Zhao,

- W. P. Xu, J. F. Liu, and H. Xu, (2016), arXiv:1611.06386.
- ¹⁹ Rui Yu, Hongming Weng, Zhong Fang, Xi Dai, and Xiao Hu, “Topological node-line semimetal and dirac semimetal state in antiperovskite Cu_3PdN ,” *Phys. Rev. Lett.* **115**, 036807 (2015).
- ²⁰ Kieran Mullen, Bruno Uchoa, and Daniel T. Glatzhofer, “Line of Dirac nodes in hyperhoneycomb lattices,” *Phys. Rev. Lett.* **115**, 026403 (2015).
- ²¹ Guang Bian, Tay-Rong Chang, Hao Zheng, Saavanth Velury, Su-Yang Xu, Titus Neupert, Ching-Kai Chiu, Shin-Ming Huang, Daniel S. Sanchez, Ilya Belopolski, Nasser Alidoust, Peng-Jen Chen, Guoqing Chang, Arun Bansil, Horng-Tay Jeng, Hsin Lin, and M. Zahid Hasan, “Drumhead surface states and topological nodal-line fermions in TiTaSe_2 ,” *Phys. Rev. B* **93**, 121113 (2016).
- ²² Brian Skinner, “Coulomb disorder in three-dimensional Dirac systems,” *Phys. Rev. B* **90**, 060202(R) (2014).
- ²³ Ya. I. Rodionov and S. V. Syzranov, “Conductivity of a Weyl semimetal with donor and acceptor impurities,” *Phys. Rev. B* **91**, 195107 (2015).
- ²⁴ Tsuneya Ando, “Screening effect and impurity scattering in monolayer graphene,” *J. Phys. Soc. Japan* **75**, 074716 (2006).
- ²⁵ E. H. Hwang and S. Das Sarma, “Dielectric function, screening, and plasmons in two-dimensional graphene,” *Phys. Rev. B* **75**, 205418 (2007).
- ²⁶ These constants of proportionality between $\Pi(\mathbf{q})$ and $|\mathbf{q}|$ are calculated for the case of a circular nodal line in Ref. 39.
- ²⁷ A. A. Abrikosov, *Fundamentals of the Theory of Metals* (Elsevier, Oxford, 1988).
- ²⁸ K. B. Efetov, *Supersymmetry in Disorder and Chaos* (Cambridge University Press, New York, 1999).
- ²⁹ A. A. Abrikosov, L. P. Gorkov, and I. E. Dzyaloshinski, *Methods of Quantum Field Theory in Statistical Physics* (Dover, New York, 1975).
- ³⁰ This transport scattering is equivalent to the scattering of electrons on the surface of a 3D topological insulator with bulk impurities.⁴⁰
- ³¹ V. F. Gantmakher, *Electrons and Disorder in Solids* (Oxford University Press, 2005).
- ³² E. McCann, K. Kechedzhi, Vladimir I. Fal’ko, H. Suzuura, T. Ando, and B. L. Altshuler, “Weak-localization magnetoresistance and valley symmetry in graphene,” *Phys. Rev. Lett.* **97**, 146805 (2006).
- ³³ I. L. Aleiner and K. B. Efetov, “A finite-temperature phase transition for disordered weakly interacting bosons in one dimension,” *Phys. Rev. Lett.* **97**, 236801 (2006).
- ³⁴ Madhab Neupane, Ilya Belopolski, M. Mofazzel Hosen, Daniel S. Sanchez, Raman Sankar, Maria Szlawska, Su-Yang Xu, Klauss Dimitri, Nagendra Dhakal, Pablo Maldonado, Peter M. Oppeneer, Dariusz Kaczorowski, Fangcheng Chou, M. Zahid Hasan, and Tomasz Durakiewicz, “Observation of topological nodal fermion semimetal phase in ZrSiS ,” *Phys. Rev. B* **93**, 201104 (2016).
- ³⁵ R. Singha, A. Pariari, B. Satpati, and P. Mandal, “Titanic magnetoresistance and signature of non-degenerate Dirac nodes in ZrSiS ,” (2016), arxiv:1602.01993.
- ³⁶ Mazhar N. Ali, Leslie M. Schoop, Chirag Garg, Judith M. Lippmann, Eric Lara, Bettina Lotsch, and Stuart Parkin, “Butterfly magnetoresistance, quasi-2D Dirac Fermi surfaces, and a topological phase transition in ZrSiS ,” (2016), arxiv:1603.09318.
- ³⁷ Michael S. Lodge, Guoqing Chang, Bahadur Singh, Jack Hellerstedt, Mark Edmonds, Dariusz Kaczorowski, Md Mofazzel Hosen, Madhab Neupane, Hsin Lin, Michael S. Fuhrer, Bent Weber, and Masahiro Ishigami, (2017), coming soon.
- ³⁸ S. V. Syzranov and L. Radzihovsky, “High-dimensional disorder-driven phenomena in Weyl semimetals, semiconductors and related systems,” (2016), arXiv:1609.05694.
- ³⁹ Yejin Huh, Eun-Gook Moon, and Yong Baek Kim, “Long-range Coulomb interaction in nodal-ring semimetals,” *Phys. Rev. B* **93**, 035138 (2016).
- ⁴⁰ Brian Skinner, Tianran Chen, and B. I. Shklovskii, “Effects of bulk charged impurities on the bulk and surface transport in three-dimensional topological insulators,” *JETP* **117**, 579 (2013).
- ⁴¹ S. Das Sarma, Shaffique Adam, E. H. Hwang, and Enrico Rossi, “Electronic transport in two-dimensional graphene,” *Rev. Mod. Phys.* **83**, 407 (2011).

Supplemental Material for “Electron transport in nodal-line semimetals”

CALCULATION OF TRANSPORT AND ELASTIC SCATTERING TIMES

In what follows we present details of the calculation of the transport and elastic scattering times, τ_{tr} and τ_0 , respectively, in both regimes of low and high doping. The transport scattering time for quasiparticles near a straight nodal line is given by

$$\frac{1}{\tau_{\text{tr}}(\varepsilon)} = \pi n_{\text{imp}} \nu_{2D}(\varepsilon) \int_{-\infty}^{\infty} \frac{dk_z}{2\pi} \int_0^{2\pi} \frac{d\theta}{2\pi} (1 - \cos^2 \theta) \left| \phi \left[\left(k_z^2 + \frac{4\varepsilon^2}{v^2} \sin^2 \frac{\theta}{2} \right)^{\frac{1}{2}} \right] \right|^2, \quad (\text{S1})$$

which follows directly from Eq. (8). The quantity $\sqrt{k_z^2 + (4\varepsilon^2/v^2) \sin^2(\theta/2)}$ in Eq. (S1) is the change in quasiparticle momentum upon scattering by an angle θ .

The elastic scattering time is given by

$$\frac{1}{\tau_0(\varepsilon)} = \pi n_{\text{imp}} \nu_{2D}(kv) \int_{-\infty}^{\infty} \frac{dk_z}{2\pi} \int_0^{2\pi} \frac{d\theta}{2\pi} (1 + \cos \theta) \left| \phi \left[\left(k_z^2 + \frac{4\varepsilon^2}{v^2} \sin^2 \frac{\theta}{2} \right)^{\frac{1}{2}} \right] \right|^2, \quad (\text{S2})$$

which differs from Eq. (S1) only by a factor $(1 - \cos \theta)$ in the integrand.

A. Low-doping regime

The scattering rate of the quasiparticles at the Fermi energy and at low temperatures depends on the details of the impurity potential at distances of order of the quasiparticle wavelength $v/|\mu|$ and, thus, on the polarisation operator at momenta of order of $k_F = |\mu|/v$. Near each small straight segment of the nodal line the motion of electrons is effectively two-dimensional, with the contribution to the polarisation operator given by the polarisation operator of 2D Dirac electrons (graphene)^{24,25,41}

$$\Pi_{2D}(\mathbf{k}) = \frac{gk_F}{2\pi v} f\left(\frac{k}{2k_F}\right), \quad (\text{S3})$$

multiplied by $dK_{\parallel}/(2\pi)$, where dK_{\parallel} is the length of the segment; \mathbf{k} is the two-dimensional momentum and $f(x)$ is a function that accounts for both interband and intra-

band electron polarisation, and is given by

$$f(x) = \begin{cases} 1, & x < 1, \\ 1 + \frac{\pi x}{4} - \frac{1}{2}\sqrt{1-x^2} - \frac{x}{2} \arcsin\left(\frac{1}{x}\right), & x > 1. \end{cases} \quad (\text{S4})$$

The polarisation function for the entire nodal line is obtained by adding up the contributions $\Pi_{2D}(\mathbf{k}_{\perp}) \cdot dK_{\parallel}/(2\pi)$ for each segment of length dK_{\parallel} , where \mathbf{k}_{\perp} is the momentum perpendicular to the segment. While the result of this addition depends in general on the shape of the nodal line, it will generally have the same functional form as $\Pi_{2D}(\mathbf{q})$ in terms of its dependence on the three-dimensional momentum \mathbf{q} for a given fixed direction of \mathbf{q} . In this paper we use the approximation of an isotropic polarisation function, so that

$$\Pi(\mathbf{q}) = \text{const} \times \Pi_{2D}(q) \frac{K_{\circ}}{2\pi}. \quad (\text{S5})$$

In terms of the constant C introduced in Eq. (3), the polarisation function can be written as

$$\Pi(\mathbf{q}) = \frac{8Cgk_F K_{\circ}}{v} f\left(\frac{q}{2k_F}\right). \quad (\text{S6})$$

The screened potential is given, in terms of the polarisation operator, is given by

$$\phi(q) = \frac{\phi_0(q)}{1 - \Pi(q)\phi_0(q)}. \quad (\text{S7})$$

Using Eqs. (S1), (S6) and (S3) and evaluating the integral numerically yields Eq. (9) with $\gamma_{\text{tr}} \approx 175C^2$.

The elastic scattering time τ_0 can be evaluated similarly, leading to Eq. (9) with the constant γ_{tr} replaced by the value $\gamma_{\text{el}} \approx 84.7C^2$.

B. High-doping regime

In the high-doping regime, corresponding to strongly screened impurities, the quasiparticle scattering is dominated by impurities far from the x - y plane of the quasiparticle motion. Since the potential of the impurities is screened exponentially, they contribute only small-momentum scattering, and therefore a typical scattering event rotates the quasiparticle momentum only by a small angle $\theta \ll 1$, as follows also directly from the integral (S1). Consequently, the transport scattering time τ_{tr} significantly exceeds the elastic scattering time τ_0 .

One can evaluate τ_{tr} using Eq. (S1) and the screened potential $\phi(q) = 4\pi e^2 / [\varkappa(q^2 + \lambda_{\text{TF}}^{-2})]$, which is the Fourier transform of Eq. (7). This calculation gives the result announced in Eq. (12). On the other hand, evaluating the elastic scattering rate using Eq. (S2) gives

$$\tau_0 = \frac{1}{4\pi\alpha^2 n_{\text{imp}} v \lambda_{\text{TF}}^2}, \quad (\text{S8})$$

as announced in the main text. This elastic scattering time is smaller than τ_{tr} by a factor $(\ln X)/X^2$, where $X = |\mu|\lambda_{\text{TF}}/v \gg 1$ in the high-doping regime.